



Obrabotka metallov -

Metal Working and Material Science









Journal homepage: http://journals.nstu.ru/obrabotka_metallov



The influence of tungsten carbide particle size on the characteristics of metalloceramic WC/Fe-Ni-Al coatings

Alexander Burkov^a, Maxim Dvornik^b, Maria Kulik^{c,*}, Alexandra Bytsura^d

Khabarovsk Federal Research Center FEB RAS, 153 Tihoockanskaya st., Khabarovsk, 680042, Russian Federation

^a  <https://orcid.org/0000-0002-5636-4669>,  burkovalex@mail.ru; ^b  <https://orcid.org/0000-0002-1216-4438>,  maxxxx80@mail.ru;
^c  <https://orcid.org/0000-0002-4857-1887>,  marijka80@mail.ru; ^d  <https://orcid.org/0009-0005-4750-7970>,  alex_btsr@mail.ru

ARTICLE INFO

Article history:

Received: 11 June 2025

Revised: 03 July 2025

Accepted: 24 July 2025

Available online: 15 September 2025

Keywords:

WC/Fe-Ni-Al coating

Electrospark depositing (ESD)

Coefficient of friction

Oxidation resistance

Wear

WC nanopowder

Funding

The work was carried out within the framework of state assignment No. 075-00399-25-04.

ABSTRACT

Introduction. The granulometry (particle size distribution) of the starting powders significantly influences the hardness and strength of compacted tungsten carbide (WC) metalloceramic materials, but this effect has not been extensively studied in the context of WC/Fe-Ni-Al coatings. **The purpose of this work** is to investigate the influence of the granulometry of the starting WC powder introduced into the non-localized electrode on the kinetics of mass transfer, chemical composition, cross-sectional microstructure of WC/Fe-Ni-Al coatings, and their corrosion and tribological properties. **Methods.** WC/Fe-Ni-Al coatings were deposited on 45 steel substrates using the electrospark deposition (ESD) method with a non-localized electrode. The electrode comprised iron granules ($\varnothing = 4$ mm), Ni and Al powders, and WC powders with varying particle sizes. X-ray diffraction (XRD) analysis revealed that the coatings consisted of tungsten carbide, tungsten semicarbide (W_2C), intermetallic phases ($Al_{66}Fe_{14}$), ferronickel (FeNi), and body-centered cubic (BCC) phases (AlNi, AlFe). **Results and discussion.** It was determined that, with an increase in the WC powder particle size fraction in the electrode, the coating matrix composition became enriched with aluminum, while the iron concentration decreased from 60 to 30 at.%. The lowest values for hardness, wear resistance, and oxidation resistance were observed for the sample obtained using WC nanopowder. The microhardness of the coating surface ranged from 4.39 to 9.16 GPa. The oxidation resistance of the coated samples at 700 °C increased monotonically with increasing WC powder particle size. The study found that the use of WC powder with a particle size fraction of 20 to 40 μ m resulted in the best performance in terms of hardness, wear resistance, and oxidation resistance of the WC/Fe-Ni-Al coatings at 700 °C. The application of these coatings increased the oxidation resistance of 45 steel by 11.6 times and wear resistance by 44 to 80 times, suggesting their potential for use in high-intensity applications.

For citation: Burkov A.A., Dvornik M.A., Kulik M.A., Bytsura A.Yu. The influence of tungsten carbide particle size on the characteristics of metalloceramic WC/Fe-Ni-Al coatings. *Obrabotka metallov (tekhnologiya, oborudovanie, instrumenty) = Metal Working and Material Science*, 2025, vol. 27, no. 3, pp. 221–235. DOI: 10.17212/1994-6309-2025-27.3-221-235. (In Russian).

Introduction

Recently, NiAl coatings have attracted attention due to their excellent resistance to high-temperature oxidation [1, 2]. The application of NiAl coatings in high-temperature environments has gained wide attention due to their ability to form a dense and stable Al_2O_3 scale [1]. It is known that the hardness, wear resistance, and compressive yield strength of NiAl-based alloys increase with an increase in iron content up to 20 at.% [3]. In the study [4], $Fe_{75}Ni_{15}Al_{10}$ and $Fe_{56}Ni_{14}Al_{30}$ coatings were obtained on the surface of low-carbon steel using the method of gas flame spraying of a mixture of iron, nickel, and aluminum powders. It has been shown that increasing the concentration of aluminum in Fe-Ni-Al coatings improves their oxidation resistance.

* Corresponding author

Kulik Maria A., Junior Researcher

Khabarovsk Federal Research Center FEB RAS,

153 Tihoockanskaya st.,

680042, Khabarovsk, Russian Federation

Tel.: +7 4212 22-69-56, e-mail: marijka80@mail.ru

At the same time, a cursory literature analysis shows that the wear resistance of *Fe-Ni-Al* composites is still significantly inferior to that of metalloceramic composites (*MMCs*). Therefore, reinforcing *Fe-Ni-Al* compositions with ceramic powder particles presents a promising strategy to significantly increase their hardness and wear resistance while maintaining high oxidation resistance.

Tungsten carbide (*WC*) is often considered as a reinforcing component of *MMCs* due to its high hardness and good wettability with metal melts [5–7]. The *Fe-Ni-Al* composition exhibits exceptionally high oxidation resistance but relatively poor wear resistance, while hard tungsten carbide is easily oxidized at high temperatures. Therefore, reinforcing the *Fe-Ni-Al* matrix with tungsten carbide allows for the creation of a *WC/Fe-Ni-Al* composite coating that combines high oxidation resistance and wear resistance.

According to a literature analysis, metalloceramic *WC/Fe-Ni-Al* coatings have previously been applied using techniques such as flame spraying [8], plasma-arc powder spraying [9], and electrospark deposition (*ESD*) [10]. Electrospark deposition (*ESD*) is a surface hardening technology that uses low-voltage, high-current electrical discharges to melt and transfer material from the working electrode to the substrate surface, significantly increasing the surface hardness and wear resistance. *ESD* technology offers notable advantages such as process simplicity, low cost, low residual stresses, and minimal substrate deformation, making it a highly effective method for producing coatings on metals and alloys [11]. The high temperature generated during the spark discharge process melts the electrode material, resulting in a uniform and dense coating, and the metallurgical bond ensures high adhesion of the coating to the substrate. The *ESD* method is employed in various applications: to improve the physical and chemical properties of metallic materials by applying refractory metals and their compounds; to expand the scope of application of composite materials by creating wear-resistant and oxidation-resistant layers on their surface; and to alter the chemical and phase composition of the surface in a controlled manner by processing in the presence of a reactive gas (e.g., nitriding of a titanium alloy) [12].

The use of a non-localized electrode (*NE*) for *ESD* facilitates the automation of the coating application process, including on curved parts, and enables the use of powders as the primary coating constituent [13]. In a previous study, *WC/Fe-Ni-Al* coatings with a high ceramic content were produced by the *ESDNE* method using a *NE* consisting of nickel and aluminum granules, and α *WC* powder with an average particle size of 1 μm [10]. In the field of compact *WC-Co* metalloceramic materials, the particle size of tungsten carbide has a significant effect on the hardness and strength of sintered products [14, 15]. However, the influence of the *WC* powder particle size on the properties of metalloceramic coatings has not been systematically investigated.

Aim of the study is to investigate the influence of the particle size distribution (granulometry) of the initial *WC* powder introduced into the non-localized electrode on the kinetics of mass transfer, chemical composition, cross-sectional structure of *WC/Fe-Ni-Al* coatings, and their corrosion and tribological properties.

To achieve the stated aim, the following **tasks** were accomplished:

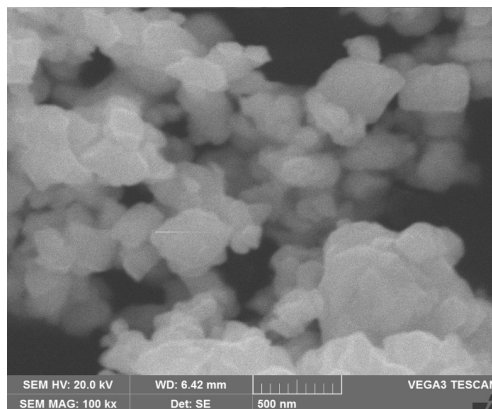
- preparation of various tungsten carbide powder fractions via grinding in a planetary ball mill and sieve analysis;
- investigation of the influence of the particle size distribution of the initial tungsten carbide powder used in a non-localized electrode on mass transfer, composition, and structure of the coating;
- establishment of the relationship between the coating's structure and its properties: roughness, wettability, hardness, wear resistance, and oxidation resistance.

Methods

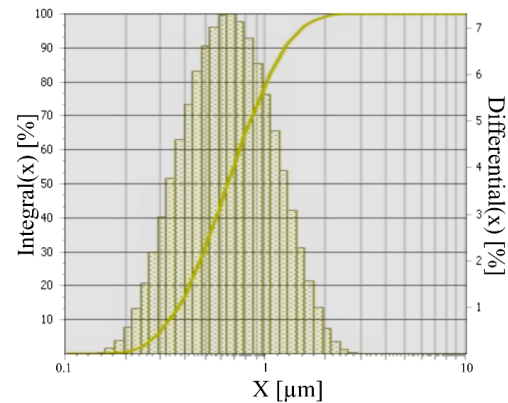
The working electrode for the *ESD* was a non-localized electrode consisting of iron granules and *Ni*, *Al* and *WC* powders (Table 1). Iron granules were obtained by cutting welding wire (*SV-08AA*) with a diameter of 4 ± 0.1 mm into cylinders with a length of 4 ± 0.5 mm. The tungsten carbide powder fractions ranged from 80 nm to 40 μm . The most dispersed fraction was nanostructured *WC* powder (99.95%) with an average particle diameter by volume D [4.3] of 0.8 μm , produced by *Hongwu* (China) (Fig. 1, *a*, *b*).

Composition of non-localized electrode and coating designations

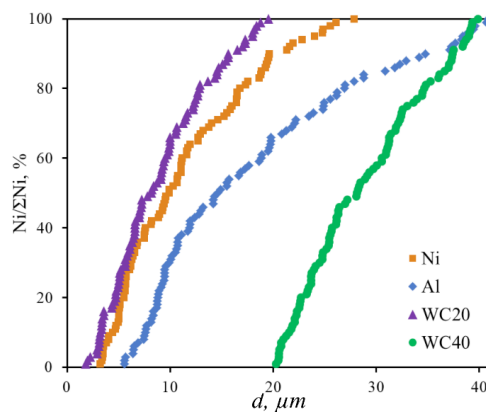
Designation of coatings	Proportion of granules, vol. %	Proportion of Al powder, vol. %	Proportion of Ni powder, vol. %	Proportion of WC powder, vol. %	WC powder fraction, μm
WCn	93.80	2.05	1.35	2.80	$0.08 \leq WC \leq 0.1$
WC20					$1 \leq WC \leq 20$
WC40					$20 \leq WC \leq 40$



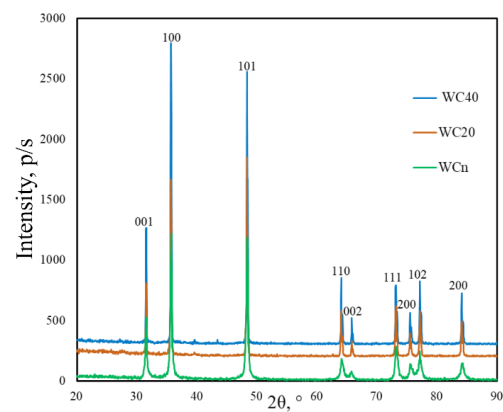
a



b



c



d

Fig. 1. SEM image of WCn fraction powder particles (a) and the results of its BET analysis (b); integral distribution of Ni, Al, WC20, WC40 powders (c) and X-ray diffraction patterns of WC powders (d)

To prepare larger fractions, WC powder (TU 6-09-03-360-78) with particle size of $1 \leq WC \leq 40 \mu\text{m}$ was used, which was separated through $40 \mu\text{m}$ and $20 \mu\text{m}$ sieves using a vibrating table. The particle diameter of the powders was measured using the arbitrary secant method according to ASTM E112-12. The average particle size of aluminum and nickel powders was $18.0 \pm 10.3 \mu\text{m}$ and $11.3 \pm 6.4 \mu\text{m}$, respectively (Fig. 1, c). X-ray diffraction (XRD) patterns revealed that as the WC particle diameter decreased, a monotonic decrease in reflection intensity and an increase in reflection width were observed, consistent with the Scherrer equation (Fig. 1, g).

The substrate (cathode), made of grade 45 steel in the form of a cylinder ($d = 12 \text{ mm}$ and $h = 10 \text{ mm}$), was immersed in a mixture of granules and powders with the end surface facing down. Thus, the coating was formed on the end and side surfaces of the substrate, with a total covered area of 2.88 cm^2 . An IMES-40 generator was used as a source of current pulses. The device settings were as follows: pulse duration – $100 \times 10^{-6} \text{ s}$, frequency – 10^3 Hz , pulse current amplitude – 170 A at an open circuit voltage of 25 V .

The coatings were applied in an argon flow at a rate of $0.3 \text{ m}^3/\text{hour}$ to protect the electrodes from oxidation. The total coating time for one sample was 10 minutes. A more detailed description of the laboratory setup for automatic coating application using the *ESDNE* method with powders is given in the study [16].

The weight gain of the substrate was measured on a laboratory scale (*Vibra HT120*) (10^{-4} g) every 120 s of *ESDNE* treatment. The phase composition of powders and prepared samples was studied by X-ray diffraction. For this purpose, a multifunctional X-ray diffractometer *DRON-7* (*NPP Burevestnik*, Russia) with $\text{Cu-K}\alpha$ radiation ($\lambda = 1.54056 \text{ \AA}$) was used in this work. For metallographic examination of the microstructure and chemical microanalysis of samples with coatings, a scanning electron microscope *Vega 3 LMH* (*Tescan*, Czech Republic) equipped with a microanalyzer (*EDS*) *X-max 80* (*Oxford Instruments*, UK) was used. The surface roughness of the coatings was measured using a 296 profilometer (*USSR*). For each sample, 10 roughness measurements were taken and average values were calculated. To determine wettability, the “sessile drop” method was used. A drop of distilled water was applied to the horizontal surface of the coating, and the contact angle with the surface at a temperature of $25 \text{ }^\circ\text{C}$ was determined from the drop profile [17]. For each sample, 5 measurements of wettability were performed, and average values were calculated. Microhardness was determined using the restored indentation method using a *PMT3-M* microhardness tester. Microhardness measurements were carried out using the Vickers method with a loading force of 1.96 N and an exposure time of 12 s. On each sample, 20 indentations were made, 20 measurements of the microhardness value were carried out, and the average values were calculated. Tests for the coefficient of friction and wear of samples were carried out using the “pin-on-disk” scheme [18–20] under a load of 25 N at speeds of 0.47 and 1.89 m/s for 10 minutes. Discs ($d = 50 \text{ mm}$) made of high-speed steel *M45* (60 HRC) were used as the counterbody. For each sample, at least 4 measurements were made, the average data sets were calculated, and the average values of the friction coefficient were determined. To determine wear resistance, at least 6 measurements were taken for each sample. To study cyclic oxidation resistance, samples of *Steel 45* and samples with coatings that had a cubic shape with a 6 mm edge were used in the experiment. The samples were kept in a muffle furnace in cycles of ~ 6 hours at a temperature of $700 \text{ }^\circ\text{C}$, and then placed in a desiccator to cool, and then weighed. The experiment was carried out for 100 hours.

Results and Discussion

When testing new compositions of non-localized electrodes, it is necessary to monitor the cathode weight gain during processing to establish the specific weight gain, as it characterizes the volume of material transferred to the substrate. Negative weight gain values indicate that a coating will not form. At the moments of voltage pulse application, electrical discharges occurred at the points of electrical contact between the granules and the substrate. This was accompanied by the transfer of metal from the melt pool of the granule to a pool on the surface of the substrate. Particles of *Ni*, *Al*, and *WC* powders located on the surface of the substrate or granules in the discharge impact area were wetted by the molten metal and incorporated into the melt pool on the substrate, forming a coating. With increasing processing time, the weight gain of the substrate gradually increased for all samples (Fig. 2, *a*). After 10 minutes of processing, the average values of the total specific weight gain of the cathode ranged from 2.74 to 4.76 mg/cm^2 , with the *WC40* sample exhibiting the minimum value. The total weight gain values for the *WCn* and *WC20* samples were very close, whereas the weight gain rate for *W40* was noticeably lower. This may be due to the low specific surface area of large particles. The low surface area results in a lower specific surface free energy, which may not be sufficient for reliable particle attachment to the granule and cathode surfaces, potentially limiting the incorporation of such particles into the coating.

X-ray diffraction (*XRD*) analysis revealed that the structure of the coatings contains tungsten carbide (*WC*), tungsten subcarbide (W_2C), body-centered cubic (*BCC*) phases, an intermetallic compound ($\text{Al}_{86}\text{Fe}_{14}$), and an *FeNi* solid solution (Fig. 2, *b*). *BCC* phases may be represented by intermetallic compounds *AlNi*

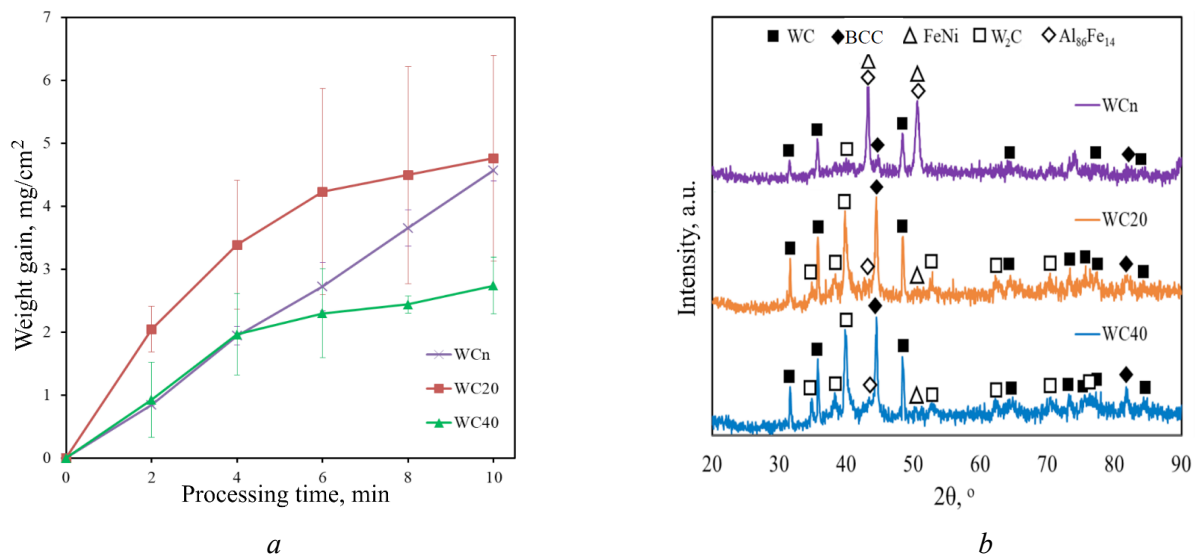


Fig. 2. Mass transfer of samples during coating deposition (a) and XRD analysis of the obtained coatings (b)

and $AlFe$, the reflections of which overlap on the 2θ scale. The W_2C phase formed as a result of tungsten carbide decarburization during interaction with molten iron in a melt pool, according to reaction 1:



Thus, the prepared coatings exhibit a metalloceramic structure, where the metal binder is composed of aluminides and ferronickel, while tungsten carbides serve as reinforcing phases. The X-ray diffraction patterns of coatings obtained using micron-sized powders differ significantly from those obtained using nanopowders. Specifically, tungsten carbide (WC) is the most abundant phase in the $WC20$ and $WC40$ coatings, whereas ferronickel and the $Al_{86}Fe_{14}$ aluminide are present in higher concentrations in the WCn coating (Table 2). Furthermore, the concentration of the W_2C phase is lowest in the WCn coating compared to the other samples.

Table 2

Results of semi-quantitative phase analysis of coatings in accordance with Fig. 2, b

Samples	Concentration, vol.%				
	WC	BCC	W_2C	$FeNi$	$Al_{86}Fe_{14}$
WCn	19.5	20.5	3.9	40	16.1
$WC20$	32.3	23.6	20.9	15.6	7.5
$WC40$	31.0	28.4	30.0	6.4	4.6

Cross-sectional images of the MMCs coatings are shown in Fig. 3, a–d. The average coating thickness was very similar, ranging from 24.3 to 26.1 μm . The coating structure consists of a $Fe-Ni-Al$ matrix and grains in the micron and submicron ranges. The Wn coating appears homogeneous without micron-sized inclusions (Fig. 3, a). At higher magnification, diamond-shaped crystallites with sizes ranging from 0.16 to 0.47 μm are observed in the Wn coating, uniformly distributed throughout the coating layer (Fig. 3, b). Given the low concentration of the W_2C phase in this coating (Fig. 2, b), it is reasonable to assume that the diamond-shaped crystallites are tungsten carbide. In the $W20$ and $W40$ coatings, both micron- and submicron-sized carbide grains are observed. Elemental mapping results reveal that the micron-sized inclusions are enriched in tungsten and carbon (Fig. 4). The difference in size and non-uniform distribution

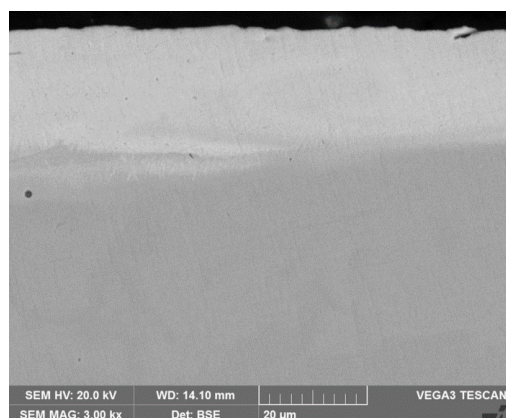
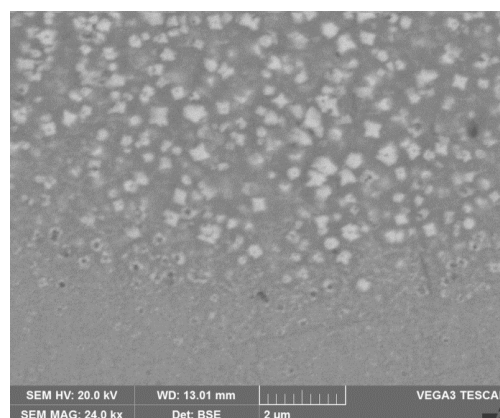
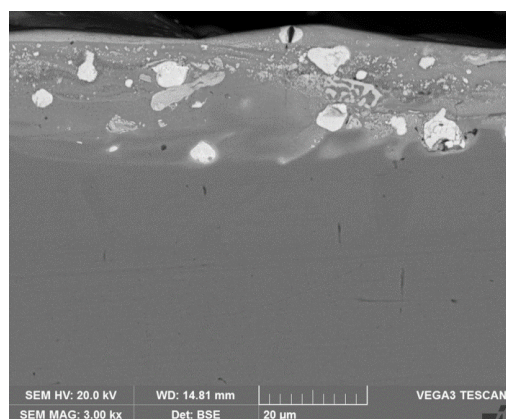
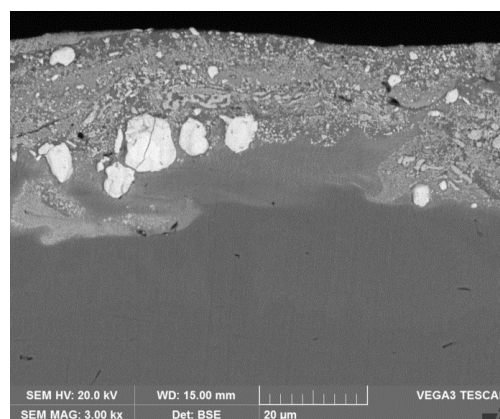
*a**b**c**d*

Fig. 3. SEM images of the cross-section of coatings: WC_n (*a*, *b*), WC_{20} (*c*) and WC_{40} (*d*)

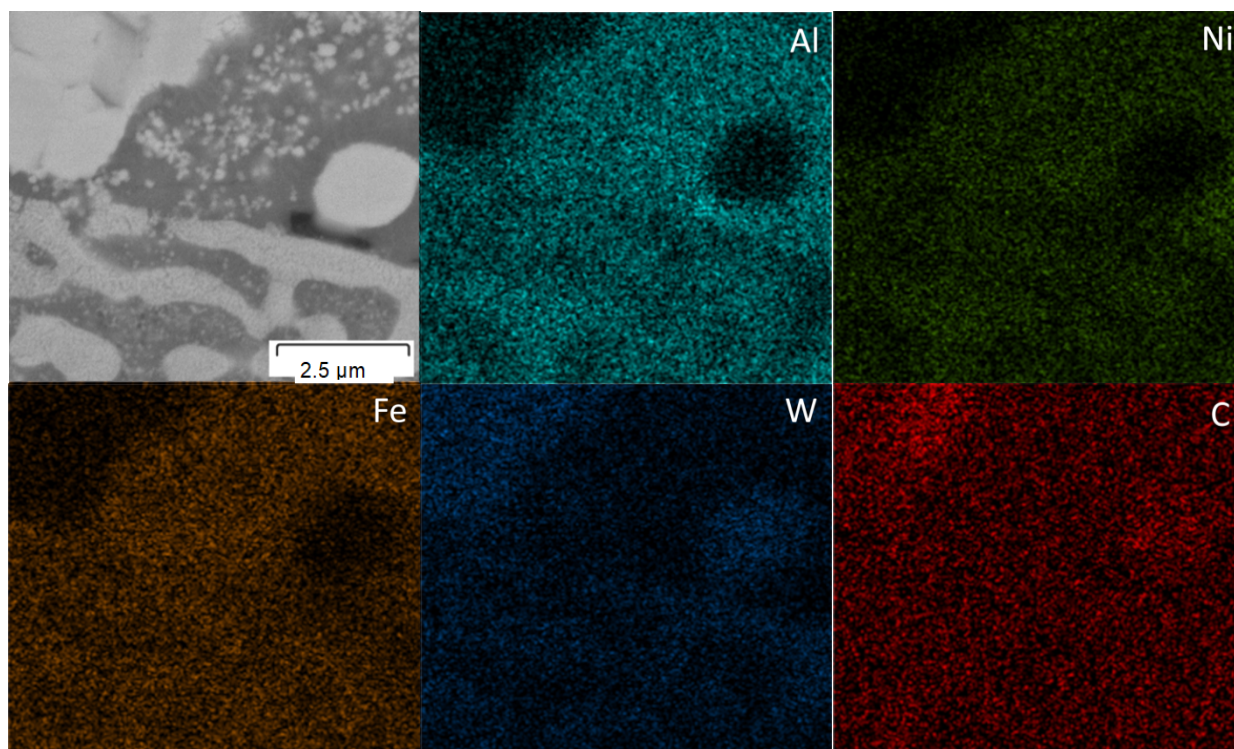


Fig. 4. Mapping of the WC_{20} coating area

of the white micron-sized inclusions in the WC_{20} and WC_{40} coatings suggest that they are original tungsten carbide WC particles. The cross-sectional images clearly show that the size of micron-sized WC inclusions increases with an increase in the WC powder fraction in the electrode. The diameter of the micron grains was smaller than the median particle diameter in the original W_{20} and W_{40} powders (Fig. 1, *c, d*). This suggests that the original powder particles were agglomerates of carbides, which disintegrated into fragments when wetted by the $Fe-Ni-Al$ melt in the discharge pool and dissolved upon interaction with iron. The submicron inclusions in Fig. 4 likely formed via WC crystallization from the melt, as they resemble the diamond-shaped inclusions of the WC_n sample, and reaction 1 is reversible. Micron inclusions could also act as WC crystallization centers, growing further during crystallization of the melt microbath after the discharge ceased. The distribution of aluminum, nickel, and iron is uniform, indicating a homogeneous composition of the coating matrix. The light grey areas in Fig. 4 are likely the result of tungsten carbide decarburization, as described in Eq. 1.

According to EDS analysis, the coatings contain tungsten, nickel, aluminum, and iron (Fig. 5, *a-c*). The source of iron is both the granules and the substrate. The concentration of elements remained relatively constant throughout the coating thickness. Fluctuations in tungsten concentration can be attributed to the presence of tungsten carbide grains in the path of the scanning electron beam. As the powder fraction size in the NE increased, the aluminum content in the coating matrix increased, while the iron (Fe) content decreased from 58 to 27 at.% (Fig. 5). The formation of the ESD coating inevitably involves the substrate as a source of iron. It is worth noting that the use of iron granules results in comparable iron concentrations in the coating to those obtained when using Ni and Al granules [10]. This can be explained by the fact

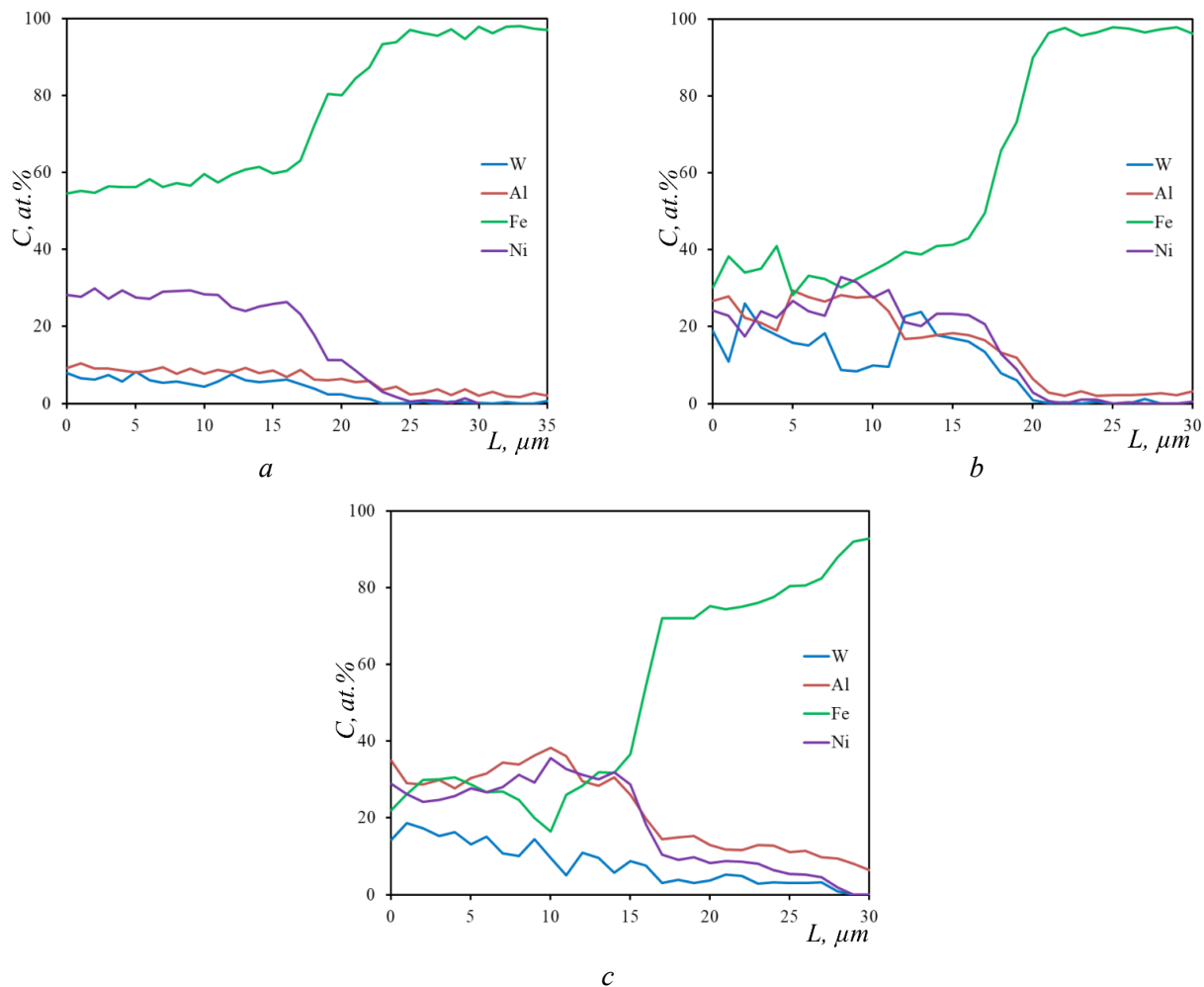


Fig. 5. Metal concentration distribution of across coating height, according to the results of EDS analysis:

a – WC_n ; *b* – WC_2 ; *c* – WC_{40}

that powders participate much more intensively in the formation of coatings during *ESDNE* compared to compact electrodes (granules).

The surface roughness (Ra) of the coated samples ranged from 5.87 to 8.23 μm (Table 3). Furthermore, the contact angle with distilled water ranged from 77.7 to 83.6°, which is significantly higher than that of *Steel 45* (54.1±1.4°). Thus, the application of *WC/Fe-Ni-Al* coatings to components made of *Steel 45* will increase the hydrophobicity of their surface due to a reduction in surface free energy. This is expected to reduce the deposition of contaminants on the surface and, consequently, limit the development of corrosion on steel structures.

Table 3

Thickness, roughness and wettability of coatings

Characteristics	Samples		
	<i>WCn</i>	<i>WC20</i>	<i>WC40</i>
Thickness, μm	25.19±5.78	24.35±5.68	26.13±6.10
Roughness, μm	8.23±2.17	6.73±0.89	5.87±0.94
Wettability, °	77.7±1.6	83.6±1.6	82.7±1.6

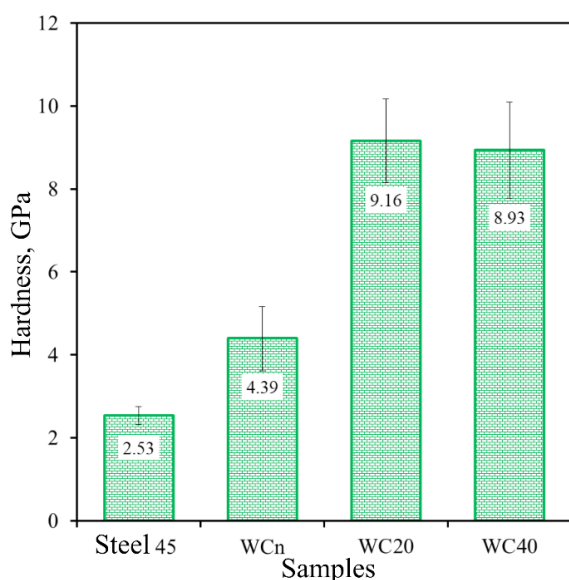


Fig. 6. Microhardness of the coating surface

The microhardness measurements on the coating surface revealed values ranging from 4.39 to 9.16 GPa, with the *WCn* sample exhibiting the minimum value and the *WC20* sample exhibiting the maximum (Fig. 6). Thus, the application of coatings allows for a 1.7 to 3.6-fold increase in the hardness of products made of *Steel 45*. The low hardness values of the sample obtained using tungsten carbide nanopowder can be attributed to the absence of large tungsten carbide inclusions in its composition. Moreover, this coating had the lowest content of the W_2C phase (30 GPa) [21]. The hardness of the *WC20* and *WC40* coatings was nearly identical, but significantly higher than that of *WCn* due to the higher content of the W_2C phase.

The results of friction tests on *WC/Fe-Ni-Al* coatings under a load of 25 N are shown in Fig. 7, *a*. During the initial 30 m of sliding, a sharp increase in friction force was observed, resulting from an increase in the contact

area between the counter-surfaces due to running-in and smoothing out of roughness asperities. The friction coefficient curves of all coatings exhibited an ascending trend in the stable stage, while the friction force values of *Steel 45* fluctuated around a constant value. This can be attributed to the increased surface roughness of the coatings (Table 3). Analysis of the friction coefficient curves revealed that the friction force noise level was significantly lower for all samples with *WC/Fe-Ni-Al* coatings compared to *Steel 45*. The average friction coefficient values of the coatings (0.73–0.83) were 6–18% lower than those of uncoated *Steel 45* (0.88). This can be attributed to the anti-friction properties of WO_3 , which forms during oxidative wear of tungsten carbide [22]. In conclusion, the use of the proposed *WC/Fe-Ni-Al* coatings allows for the reduction and stabilization of the friction coefficient of components made of *Steel 45*.

The wear resistance of the coatings was investigated at linear sliding speeds of 0.47 and 1.9 m/s under a load of 25 N. The wear rate of *WC/Fe-Ni-Al* coatings ranged from 0.61×10^{-6} to $10.91 \times 10^{-6} \text{ mm}^3/\text{Nm}$ at a speed of 0.47 m/s and from 0.30×10^{-6} to $2.70 \times 10^{-6} \text{ mm}^3/\text{Nm}$ at a speed of 1.89 m/s (Fig. 7, *b*). Therefore, the wear resistance of the developed coatings was 5 to 80 times greater than that of the

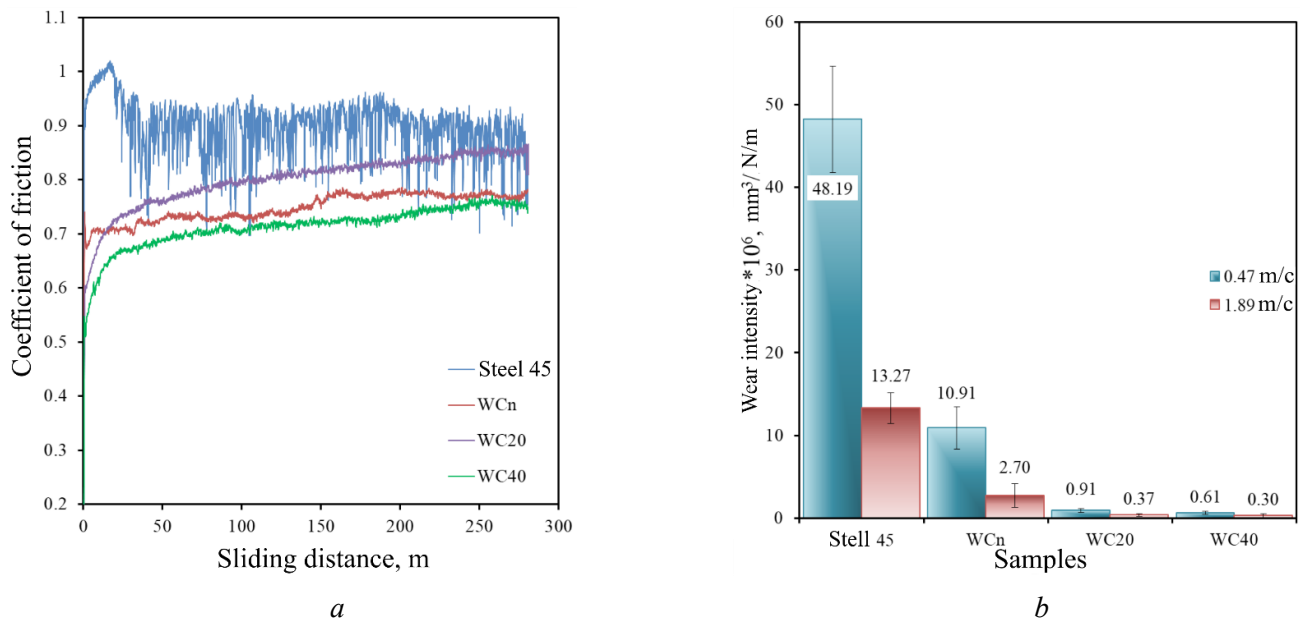


Fig. 7. Coefficient of friction at a sliding speed of 0.47 m/s and wear rate of coatings at 0.47 and 1.89 m/s

original *Steel 45*. At a sliding speed of 0.47 m/s, the wear of the samples was higher than at a higher speed (1.89 m/s). This can be attributed to the formation of a self-lubricating tribo-oxide layer, resulting from the high instantaneous temperature reached in the friction zone at the higher sliding speed [23, 24]. At both speeds, the *WCn* coating exhibited the lowest wear resistance, while the *WC40* coating exhibited the highest. The high wear resistance of the *WC40* coating can be attributed to the presence of large *WC* inclusions and areas with their accumulation, which prevented the counterbody from interacting with the abraded metal matrix of the coating.

Based on the weight gain plots of *WC/Fe-Ni-Al* coatings and *Steel 45* at 700 °C, after 100 hours of testing, the weight gain of coated samples ranged from 37.0 to 133.8 g/m², while that of uncoated *Steel 45* was 429.2 g/m² (Fig. 8, *a*). The weight gain of the coated samples increased with increasing powder dispersion, increasing by 2.6 times when transitioning from the *WC20* sample to the *WCn* sample. Thus, the results indicate that decreasing the diameter of tungsten carbide particles reduces the oxidation resistance of the *WC/Fe-Ni-Al* composition. This may be due to the increased decarburization of *WC* particles with an increase in their specific surface area, leading to a greater introduction of *W* and *C* elements into the

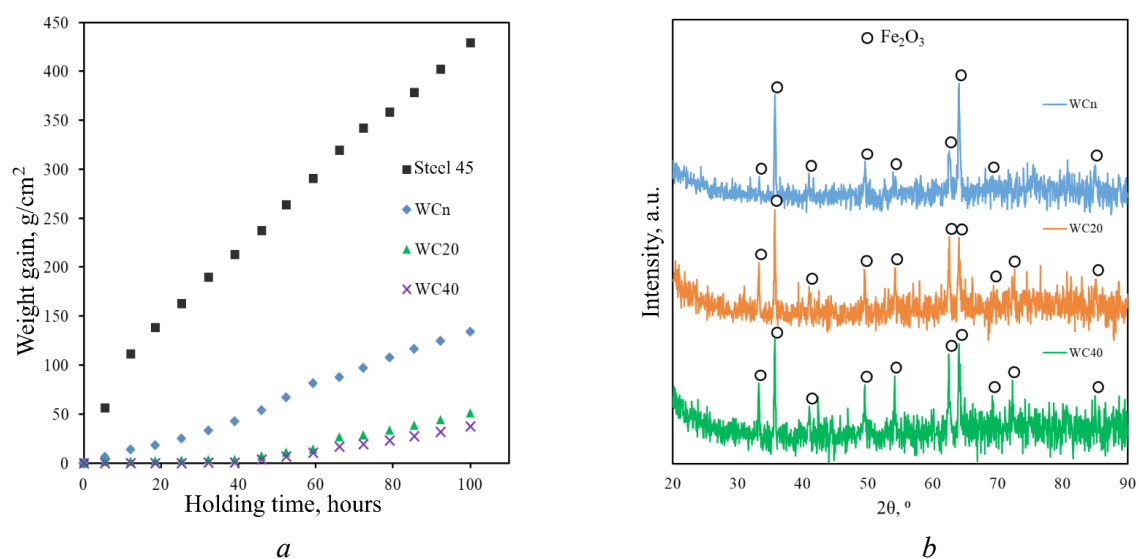


Fig. 8. Graphs of weight gain of *WC/Fe-Ni-Al* coatings and 45 steel over time at a temperature of 700 °C (*a*) and XRD patterns of coatings after oxidation resistance testing (*b*)

Fe-Ni-Al matrix, thereby reducing the barrier properties of the aluminum oxide layer formed during high-temperature oxidation. The weight gain during the oxidation resistance test results from the fixation of oxygen on the surface of the samples in the form of hematite Fe_2O_3 (Fig. 8, b). In general, the *WC20* and *WC40* composite coatings demonstrated high oxidation resistance at 700 °C. Their use allows for an 8.4 to 11.6-fold increase in the oxidation resistance of components made of *Steel 45*.

Conclusions

1. For the first time, the influence of tungsten carbide powder particle size distribution on the production of *WC/Fe-Ni-Al* metalloceramic coatings on *Steel 45* using electrospark deposition with a non-localized electrode was investigated. Tungsten carbide powder fractions of $1 \leq WC \leq 20 \mu m$ and $20 \leq WC \leq 40 \mu m$ were prepared via grinding in a planetary ball mill and subsequent sieve analysis.

2. The total weight gain values for samples *WCn* and *WC20* were similar, while the weight gain rate was noticeably lower for *W40*. X-ray diffraction analysis revealed that the deposited coatings consisted of tungsten carbide, tungsten subcarbide (W_2C), iron aluminide ($Al_{86}Fe_{14}$), ferronickel (*FeNi*), and *BCC* phases (*AlNi*, *AlFe*). It was shown that increasing the *WC* powder fraction size in the electrode resulted in enrichment of the coating matrix with aluminum, while the iron concentration decreased from 60 to 30 at.%. The coating structure corresponds to a metalloceramic composite.

3. The surface roughness of the coatings ranged from 5.87 to 8.23 μm , with a minimum value for the *WC40* sample. The contact angle of the coatings ranged from 77.7 to $83.6 \pm 1.6^\circ$, with the lowest value observed for the sample produced using tungsten carbide nanopowder.

4. The microhardness of the coating surface ranged from 4.39 to 9.16 GPa, with the lowest value observed for the sample produced using tungsten carbide nanopowder.

5. This study demonstrated that tungsten carbide particle fractions ranging from 20 to 40 μm provide the best wear resistance and oxidation resistance of *WC/Fe-N-Al* coatings at 700 °C. It was shown that the use of such coatings increases the oxidation resistance of *Steel 45* by up to 11.6 times and the wear resistance by 44 to 80 times.

References

1. Wang X., Liu Z., Cheng K., Li J., Ning H., Mao J. High-temperature corrosion characterization of Ni-Al laser cladding: The effect of Al content and Fe. *Journal of Thermal Spray Technology*, 2024, vol. 33 (5), pp. 1417–1439. DOI: 10.1007/s11666-024-01782-8.
2. Wang Z., Zhang J., Zhang F., Qi C. Study on the microstructure and properties of a laser cladding Fe–Ni–Al coating based on the invar effect. *Scientific Reports*, 2024, vol. 14 (1), p. 11685. DOI: 10.1038/s41598-024-62306-6.
3. Munroe P.R., George M., Baker I., Kennedy F.E. Microstructure, mechanical properties and wear of Ni–Al–Fe alloys. *Materials Science and Engineering: A*, 2002, vol. 325 (1–2), pp. 1–8. DOI: 10.1016/S0921-5093(01)01403-4.
4. Datu-Maki A.S.I., Ciswandi, Hermanto B., Saptari S.A., Sudiro T. Structure and oxidation resistance of flame sprayed Fe–Ni–Al coating. *Journal of Physics: Conference Series*, 2019, vol. 1204 (1), p. 012128. DOI: 10.1088/1742-6596/1204/1/012128.
5. Manikandan R., Ponnusamy P., Nanthakumar S., Gowrishankar A., Balambica V., Girimurugan R., Mayakannan S. Optimization and experimental investigation on AA6082/WC metal matrix composites by abrasive flow machining process. *Materials Today: Proceedings*, 2023. DOI: 10.1016/j.matpr.2023.03.274.
6. Alidokht S.A., Wu L., Bessette S., Chromik R.R. Microstructure and tribology of cold spray additively manufactured multimodal Ni-WC metal matrix composites. *Wear*, 2024, vol. 538, p. 205218. DOI: 10.1016/j.wear.2023.205218.
7. Liao Z., Huang X., Zhang F., Li Z., Chen S., Shan Q. Effect of WC mass fraction on the microstructure and frictional wear properties of WC/Fe matrix composites. *International Journal of Refractory Metals and Hard Materials*, 2023, vol. 114, p. 106265. DOI: 10.1016/j.ijrmhm.2023.106265.
8. Yuan J., Wang Q., Liu X., Lou S., Li Q., Wang Z. Microstructures and high-temperature wear behavior of NiAl/WC-Fe_x coatings on carbon steel by plasma cladding. *Journal of Alloys and Compounds*, 2020, vol. 842, p. 155850. DOI: 10.1016/j.jallcom.2020.155850.



9. Abreu-Castillo H.O., d'Oliveira A.S.C.M. Challenges of nanoparticle-reinforced NiAl-based coatings processed by in situ synthesis of the aluminide. *The International Journal of Advanced Manufacturing Technology*, 2024, vol. 134 (3–4), pp. 1547–1561. DOI: 10.1007/s00170-024-14162-x.
10. Burkov A.A. Use of Ni and Al granules and WC powder for electric spark deposition of metalloceramic coatings. *Izvestiya vysshikh uchebnykh zavedenii. Poroshkovaya metallurgiya i funktsional'nye pokrytiya = Powder Metallurgy and Functional Coatings*, 2025, vol. 19, no. 2, pp. 62–72. DOI: 10.17073/1997-308X-2025-2-62-72.
11. Barile C., Casavola C., Pappaletta G., Renna G. Advancements in electrospark deposition (ESD) technique: A short review. *Coatings*, 2022, vol. 12 (10), p. 1536. DOI: 10.3390/coatings12101536.
12. Nikolenko S.V., Verkhoturov A.D. *Novye elektrodnye materialy dlya elektroiskrovogo legirovaniya* [New electrode materials for electrospark alloying]. Vladivostok, Dal'nauka Publ., 2005. 219 p. ISBN 5-80444-0404-0.
13. Burkov A.A., Kulik M.A. Wear-resistant and anticorrosive coatings based on chrome carbide Cr_7C_3 obtained by electric spark deposition. *Protection of Metals and Physical Chemistry of Surfaces*, 2020, vol. 56, pp. 1217–1221. DOI: 10.1134/s2070205120060064.
14. Dvornik M., Mikhailenko E. The influence of the rotation frequency of a planetary ball mill on the limiting value of the specific surface area of the WC and Co nanopowders. *Advanced Powder Technology*, 2020, vol. 31 (9), pp. 3937–3946. DOI: 10.1016/j.apt.2020.07.033.
15. Dvornik M.I., Zaytsev A.V. Research of surfaces and interfaces increasing during planetary ball milling of nanostructured tungsten carbide/cobalt powder. *International Journal of Refractory Metals and Hard Materials*, 2013, vol. 36, pp. 271–277. DOI: 10.1016/j.ijrmhm.2012.10.004.
16. Burkov A.A. Production amorphous coatings by electrospark treatment of steel 1035 in a mixture of iron granules with CrMoWCBSi powder. *Obrabotka metallov (tekhnologiya, oborudovanie, instrumenty) = Metal Working and Material Science*, 2019, vol. 21, no. 4, pp. 19–30. DOI: 10.17212/1994-6309-2019-21.4-19-30. (In Russian).
17. Li Y.C., Zhang W.W., Wang Y., Zhang X.Y., Sun L.L. Effect of spray powder particle size on the bionic hydrophobic structures and corrosion performance of Fe-based amorphous metallic coatings. *Surface and Coatings Technology*, 2022, vol. 437, p. 128377. DOI: 10.1016/j.surfcoat.2022.128377.
18. Almond E.A., Gee M.G. Results from a UK interlaboratory project on dry sliding wear. *Wear*, 1987, vol. 120 (1), pp. 101–116. DOI: 10.1016/0043-1648(87)90136-0.
19. Kennedy F.E., Lu Y., Baker I. Contact temperatures and their influence on wear during pin-on-disk tribotesting. *Tribology International*, 2015, vol. 82, pp. 534–542. DOI: 10.1016/j.triboint.2013.10.022.
20. Nataraja M., Balakumar G., Santhosh N., Naik M.R. Characterization of wear rate of Al-12 wt% Si alloy based MMC reinforced with ZrO_2 particulates. *Materials Research Express*, 2024, vol. 11 (3), p. 036522. DOI: 10.1088/2053-1591/ad3468.
21. Chivavibul P., Watanabe M., Kuroda S. Effect of microstructure of HVOF-sprayed WC-Co coatings on their mechanical properties. *Thermal Spray*, 2007, p. 1212. DOI: 10.31399/asm.cp.itsc2007p0297.
22. Greenwood O.D., Moulzolf S.C., Blau P.J., Lad R.J. The influence of microstructure on tribological properties of WO_3 thin films. *Wear*, 1999, vol. 232 (1), pp. 84–90. DOI: 10.1016/S0043-1648(99)00255-0.
23. Jayashree P., Turani S., Straffellini G. Effect of velocity and temperature on the dry sliding behavior of a SiC-Graphite composite against WC-CoCr and WC-FeCrAlY HVOF coatings. *Wear*, 2021, vol. 464, p. 203553. DOI: 10.1016/j.wear.2020.203553.
24. Ameen H.A., Hassan K.S., Mubarak E.M.M. Effect of loads, sliding speeds and times on the wear rate for different materials. *American Journal of Scientific and Industrial Research*, 2011, vol. 2 (1), pp. 99–106. DOI: 10.5251/ajsir.2011.2.1.99.106.

Conflicts of Interest

The authors declare no conflict of interest.

© 2025 The Authors. Published by Novosibirsk State Technical University. This is an open access article under the CC BY license (<http://creativecommons.org/licenses/by/4.0>).

